Charge Density Distribution in the "Proton Sponge" Compound 1,8-Bis(dimethylamino)naphthalene

Paul R. Mallinson,*,† Krzysztof Woźniak,‡ Chick C. Wilson,§ Kirsty L. McCormack,† and and Dmitrii S. Yufit†

Contribution from the Chemistry Department, University of Glasgow, Glasgow G12 8QQ, U.K., Chemistry Department, University of Warsaw, 02-093 Warszawa, ul. Pasteura 1, Poland, and ISIS Facility, Rutherford Appleton Laboratory, Chilton, Didcot OX11 OQX, U.K.

Received September 23, 1998. Revised Manuscript Received January 19, 1999

Abstract: This is the first low-temperature, high-resolution X-ray and neutron diffraction study of charge distribution in an uncomplexed proton sponge compound. In the parent compound of this class, 1,8-bis-(dimethylamino)naphthalene (DMAN), a small degree of asymmetry of the naphthalene moiety is induced by weak, asymmetric intermolecular interactions. The only manifestation of this asymmetry is at the level of the Laplacian of the charge distribution. Comparing the DMAN molecule with its cation shows the consequences of protonation, such as shortening of the C−C, and lengthening of the C(ar)−H and C−N bond lengths. These changes are even more apparent in CP properties, with ρ_b on average smaller in the cation than in the neutral molecule. Relationships between CP and structural parameters viz. ρ_b *vs* Laplacian, Laplacian *vs* bond length, and ρ_b *vs* bond length depend on bond type, and are different for DMAN and its cation. Comparison with ab initio calculated values reveals some systematic discrepancies. Only two critical points are located between stacked DMAN molecules. Curved interaction lines joining these molecules can be associated with CH···π-electron interactions.

Introduction

The title compound DMAN (Scheme 1) belongs to the class of compounds with extremely high basicity constants and proton affinities, well known as Proton Sponges.[1,2] These compounds have already attracted considerable attention. With mineral or organic acids, proton sponges form very stable ionic complexes containing asymmetric intramolecular [N−H···N]$^+$ hydrogen bonds.[3−16]

Scheme 1

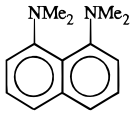

Neutrons are an excellent probe for studying both the structure and dynamics of the condensed state.[17−19] The purpose of the neutron part of this work is to determine as precisely as possible the positions of atoms and their thermal parameters in 1,8-bis-(dimethyl-amino)naphthalene [DMAN]. This is crucial information for experimental charge density studies of this parent proton sponge.

According to the X-ray structure of DMAN[20,21] the symmetric DMAN molecule is located in a general position in the orthorhombic $P2_12_12_1$ space group, thus being influenced by weak and asymmetric interactions with the crystal lattice. This is not observed at the level of structural parameters. However, these weak interactions are strong enough to differentiate solid state CP/MAS ^{13}C NMR chemical shifts of almost symmetrically located carbon nuclei[22−25] as well as the NQR peaks of

* Author for correspondence. Fax: +44(141) 330-4888. E-mail: paul@chem.gla.ac.uk.

† University of Glasgow.

‡ University of Warsaw.

§ Rutherford Appleton Laboratory.

(1) Staab, H. A.; Saupe, T. *Angew. Chem., Int. Ed. Engl.* **1988**, *27*, 865.

(2) Alder, R. W. *Chem. Rev.* **1989**, *89*, 1215.

(3) Truter, M. R.; Vickery, B. L. *J. Chem. Soc., Dalton Trans.* **1972**, 395.

(4) Pyzalska, D.; Pyzalski, R.; Borowiak, T. *J. Crystallogr. Spectrosc. Res.* **1983**, *13*, 211.

(5) Glowiak, T.; Malarski, Z.; Sobczyk, L.; Grech, E. *J. Mol. Siruct.* **1987**, *157*, 329.

(6) Wozniak, K.; Krygowski, T. M.; Kariuki, B.; Jones, W.; Grech, E. *J. Mol. Struct.* **1990**, *240*, 111.

(7) Bartoszak, E.; Jaskólski, M.; Grech, E.; Gustafsson, T.; Olovsson, I. *Acta Crystallogr.* **1994**, *B50*, 358.

(8) Miller, P. K.; Abney, K. D.; Rappe, A. K.; Anderson, O. P.; Strauss, S. H. *Inorg. Chem.* **1988**, *27*, 2255.

(9) Brown, D. A.; Clegg, W.; Colquhoun, H. M.; Daniels, J. A.; Stephenson, J. R.; Wade, K. *J. Chem. Soc., Chem. Commun.* **1987**, 889.

(10) Kanters, J. A.; Schouten, A.; Kroon, J.; Grech, E. *Acta Crystallogr.* **1991**, *C47*, 807.

(11) Kellett, P. J.; Anderson, O. P.; Strauss, S. H.; Abney, K. D. *Can. J. Chem.* **1989**, 67, 2023.

(12) Bartoszak, E.; Dega-Szafran, Z.; Grunwald-Wyspianska, M.; Jaskólski, M.; Szafran, M. *J. Chem. Soc., Faraday Trans.* **1993**, *89*, 2085.

(13) Malarski, Z.; Lis, T.; Grech, E.; Nowicka-Scheibe, J.; Majewska, K. *J. Mol. Struci.* **1990**, *221*, 27.

(14) Woźniak, K.; Wilson, C. C.; Knight, K. S. Jones, W.; Grech, E. *Acta Cryst.* **1996**, *B52*, 691.

(15) Woźniak, K.; He, H.; Klinowski, J.; Barr, T. L.; Milart, P. *J. Phys. Chem.* **1996**, *100*, 11420.

(16) Woźniak, K.; He, H.; Klinowski, J.; Jones, W.; Barr, T. L. *J. Phys.. Chem.* **1995**, *99*, 14667.

(17) Willis, B. T. M. *Thermal Neutron Diffraction*; Oxford University Press: U.K., 1970.

(18) Windsor, C. G. *Pulsed Neutron Scattering*; Taylor & Francis Ltd.: London, U.K., 1981.

(19) Bacon, G. E. *Neutron Diffraction*; Clarendon Press: Oxford, U.K., 1975.

(20) Einspahr, H.; Robert, J-B.; Marsh, R. E.; Roberts, J. D. *Acta Crystallogr.* **1973**, *B29*, 1611.

(21) Woźniak, K.; He, H.; Klinowski, J.; Nogaj, B.; Lemanski, D.; Hibbs, D.; Hursthouse M.; Howard, S. T. *J. Chem. Soc., Faraday Trans.* **1995**, *91*, 3925.

10.1021/ja983393z CCC: $18.00
Published on Web 05/01/1999

nitrogens.[25] From the point of view of charge density studies, the DMAN structure is a quite demanding test to show how sensitive are the charge density parameters for the weakest asymmetric interactions (mainly weak C−H···π-electron hydrogen bonds between the methyl groups and aromatic parts of neighboring molecules).

This is also a continuation of our previous charge density studies of the DMAN complex with 2,3-dichloromaleic acid.[26] Direct comparison of charge density data for the DMAN diamine and its complex will allow us to estimate the consequences of asymmetric protonation and formation of strong $[N-H\cdots N]^+$ hydrogen bonds in proton sponges. This could be a verification in the solid phase of the results of ab iniiio molecular orbital calculations for the isolated molecule.[27,28] The isolated DMAN molecule was also studied with ab initio methods from the point of view of estimation of the nitrogen lone pair strain contribution to its basicity.[29] An interesting phenomenon is reported[30] where two ground-state minima on the potential surface of DMAN have been found by both fluorescence and ab initio methods. The solid-state results for DAMN seem to be closer to the more symmetric DMAN moiety obtained in ref 30.

Both this work and the earlier study of the protonated cation are based respectively on equivalent neutron diffraction experiments. For uncomplexed DMAN, the neutron experiment is reported in this paper, together with the X-ray charge density results. For $DMANH^+$, the neutron diffraction structure[14] was reported prior to the X-ray charge density study.[26]

Experimental Section

DMAN crystals were recrystallized from acetonitrile by slow evaporation, as colorless prisms. Single-crystal, high-resolution X-ray diffraction data were collected on a CAD4 diffractometer using graphite-monochromated Mo Kα radiation. The crystal was cooled by a stream of cold nitrogen gas from an Oxford Cryosystems cryostream cooler. Data reduction was carried out with the DREAM suite of programs,[31] including an analytical absorption correction computed with ABSORB.[32] The intensities of standard reflections were fitted to cubic polynomials, which were used for scaling the data. Corrections were made for absorption by the crystal, but not for thermal diffuse scattering. The range of corrections, the agreement factor for the averaging of equivalent reflections, crystal data, and other experimental details are summarized in Table 1.

Multipole Refinement. The refinement minimized the function $\sum w(|F_o| - K|F_c|)^2$, where $w = 1/\sigma^2(F) = 4F^2/\sigma^2(F^2)$; $\sigma^2(F^2)$; $\sigma^2(F^2) = \sigma^2_{counting}(F^2) + P^2F^4$. The instrumental instability factor P was estimated from errors in the time-dependent scaling polynomials and the fluctuations of the standards. Anisotropic temperature factors were used to describe the thermal motion of all atoms. For hydrogen atoms, positional and thermal parameters obtained from refinement with neutron diffraction data were used. Scattering factors for C, H, and N were derived from wave functions tabulated in ref 33. The program XDLSM (described in our earlier paper[26]) of the package XD[34] was used for the multipole refinement, in which the expansion was truncated at the octapole level ($l_{max} = 3$) for carbon and nitrogen atoms, and at the dipole level ($l_{max} = 1$) for all hydrogen atoms. A single, bond-

Table 1. Experimental X-ray and Neutron Data for 1,8-Bis(dimethylamino)naphthalene

formula	$C_{14}H_{18}N_2$
molecular weight	214.31
space group (orthorhombic)	$P2_12_12_1$
temperature/K	100(5)
unit cell dimensions/Å	
a	12.781(1)
b	10.018(1)
c	9.509(1)
V/Å^3	1217.5(2)
Z	4
D_c/g cm^{-3}	1.169
F(000)	248
crystal dimensions/mm	0.5 × 0.4 × 1.0
absorption coefficient/cm^{-1}	0.65
range of corrections for absorption by crystal	0.967−0.991
radiation	Mo K_α; $\lambda = 0.7107$ Å
scan type	$\theta - 2\theta$
$(\sin\theta/\lambda)_{max}$/Å^{-1}	1.123
(*hkl*) lower limit−upper limit	−18 27; −9 22; −20 21
time period/h	419
no. of standard reflections	4 ($\bar{1}$ 2 2, $\bar{1}$ $\bar{1}$ 4, 2 $\bar{4}$ 1, 3 $\bar{2}$ 1)
no. of reflections measured	16453
no. of symmetry-independent reflections	8375
no. of $I > 2\sigma(I)$ reflections	4241
no. of symmetry-related and repeated reflections	3876
agreement factor $R = \sum\|I - \bar{I}\|/\sum I$	0.027
refined on	*F*
R	0.0279
R_w	0.0316
S	1.03
N_{obs}/N_{var}	9.6
weighting scheme	$w = 1/\sigma^2(F) = 4F^2/\sigma^2(F^2)$ $\sigma^2(F^2) = \sigma^2_{counting}(F^2) + P^2F^4$
positional and thermal parameters for H atoms taken from refinement with neutron data.	
range of residual density in asymmetric unit/eÅ^{-3}	−0.18−0.24
collection method (and site) for neutron diffraction	time-of-flight Laue diffraction, instrument SXD, ISIS pulsed neutron source (RAL, UK)
neutron wavelength	0.5−5 Å
temperature/K	100
crystal size	3 × 2 × 2 mm
θ range for neutron data collection	1.45−45.63°
$\sin\theta/\lambda_{max}$/Å^{-1} for neutron data collection	
for $\lambda = 0.7107$ Å	1.006
(*hlk*) lower limit-upper limit	0 50; 0 36;0 32
refinement method for neutron data	full-matrix least-squares on F^2
no. of reflections measured	11934
agreement factor $R = \sum\|I - \bar{I}\|/\sum I$	0.069
no. of symmetry-independent reflections	3005
no. of $I > 2\sigma(I)$ reflections	2326
$R[I > 2\sigma(I)]$	0.0707
R_w	0.1372
S	1.074
no. of restraints	0
no. of variables	307
weighting scheme	$w = 1/[\sigma^2(F_o^2) + (0.0958P)^2 + 7.08P]$ where $P = (Max(F_o^2, 0) + 2F_c^2)/3$

(22) Woźniak, K.; He, H.; Klinowski, J.; Jones, W.; Grech, E. *J. Phys. Chem.* **1994**, *98*, 13755.
(23) Woźniak, K.; He, H.; Klinowski, J.; Grech, E. *J. Phys. Chem.* **1995**, *99*, 1403.
(24) Woźiak, K. *J. Mol. Struct.* **1996**, *374*, 227.
(25) Nogaj, B.; Woźniak, K.; Lemanski, D.; Ostafin, M.; Grech. E. *Solid State NMR* **1995**, 4, 187.
(26) Mallinson, P.R.; Woźniak, K.; Smith, G. T.; McCormack, K. L. *J. Amer. Chem. Soc.* **1997**, *119*, 11502.
(27) Platts, J. A.; Howard, S. T.; Woźniak, K. *J. Org. Chem.* **1994**, *59*, 4647.
(28) Perakyla, M. *J. Org. Chem.* **1996**, *61*, 7420.
(29) Howard, S.; Platts, J. A. *J. Org. Chem.* **1998**, *63*, 3568.
(30) Szemik-Hojniak, A.; Zwier, J.M.; Buma, W.J.; Bursi, R.; van der Waals, J. H. *J. Amer. Chem. Soc.* **1998**, *120*, 4840.
(31) Blessing, R. H. *J. Appl. Cryst.* **1989**, *22*, 396 and references therein.
(32) DeTitta, G. *Computer program ABSORB,* Medical Foundation of Buffalo, Buffalo, NY, 1984.

directed dipole was used. Since all atoms are in general positions, the space group symmetry places no restrictions on the allowed multipole functions. Separate κ', κ'' were employed for aromatic C, methyl C, N, and H. Their values were allowed to vary, except those relating to H which were fixed at 1.2.

Coordinates and anisotropic displacement parameters for the hydrogen atoms only were fixed at the values obtained from a neutron diffraction experiment carried out at the same temperature (100 K), described below. We found no systematic difference between the displacement parameters for the non-H atoms obtained by X- ray and neutron diffraction. It was therefore not necessary to apply any correction to the parameters of the hydrogen atoms (see ref 35.)

Neutron Diffraction Data Collection and Refinement. Neutron measurements were made using the time-of-flight Laue diffraction (tofLD) technique. The crystal, of dimension $3 \times 2 \times 2$ mm^3, was mounted on a two-circle orienter (ϕ, χ) in a Displex closed-cycle refrigerator (CCR) helium cryostat, on the single-crystal diffractometer SXD at the ISIS spallation neutron source.[36] The data were collected at a temperature of 100 ± 1 K, the computer-controlled temperature being measured by a Rh−Fe thermocouple sited around 10 mm from the sample at the CCR head.

In this experiment, two position-sensitive detectors, each of 192×192 mm^2 active area, in 3×3 mm pixels, were used. These were situated with their centers at $2\theta = 55°$, 190 mm from the sample (low-angle detector), and $2\theta = 125°$, 150 mm from the sample (high-angle detector). The wavelength range used was 0.5−5 Å. Typical frame exposure times were around 5−6 hours, resulting in several hundred observed reflections in each detector.

Reflection intensities were extracted using standard SXD procedures, and normalized to the incident beam using the incoherent scattering from a polycrystalline vanadium sample. Semi-empirical absorption corrections were also applied at this stage, using the vanadium and sample scattering. The resulting intensities were reduced to structure factors. These data were used in the CCSL[37] least-squares refinement program SFLSQ, to apply a variable wavelength extinction correction based on the Becker−Coppens formalism[38] using a Gaussian model with one variable parameter, the mosaic spread. The resulting corrected structure factors were merged and subjected to initial refinements in the GSAS program[39] before final refinement proceeded in SHELX as described below. The total observed data set of 11 934 reflections resulted in 3005 unique, merged reflections to be used in the final refinements. The data were refined using SHELXL-93.[40] The starting parameters for the atoms were taken from an earlier low-temperature X-ray diffraction study.[21] The scattering lengths ($b_C = 6.646$, $b_H = -3.739$, and $b_N = 9.360$ fm) were taken from ref 41.

In the refinements with SHELXL-93, weighted R factors wR and all goodness-of-fit S values are based on F^2. Conventional R factors are based on F with F set to zero for negative F^2. The criterion $F > 2\sigma(F)$ was used only for calculating R factors and is not relevant to the choice of reflections for the refinement.

Results

The crystal data and a summary of the data collection and refinement parameters for DMAN are shown in Table 1, together with the final R factors and goodness of fit for the 4241 X-ray reflections used in the multipole refinement. Atom labeling is shown in Figure 1. Residual densities in a plane defined by C3, C6, and C9 are shown in Figure 2. The range of residual density values over the whole asymmetric unit is given in Table 1.

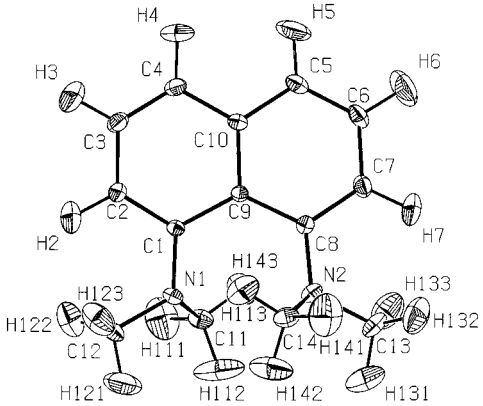

Figure 1. Anisotropic displacement ellipsoids, drawn at 50% probability, showing the labeling of the atoms.

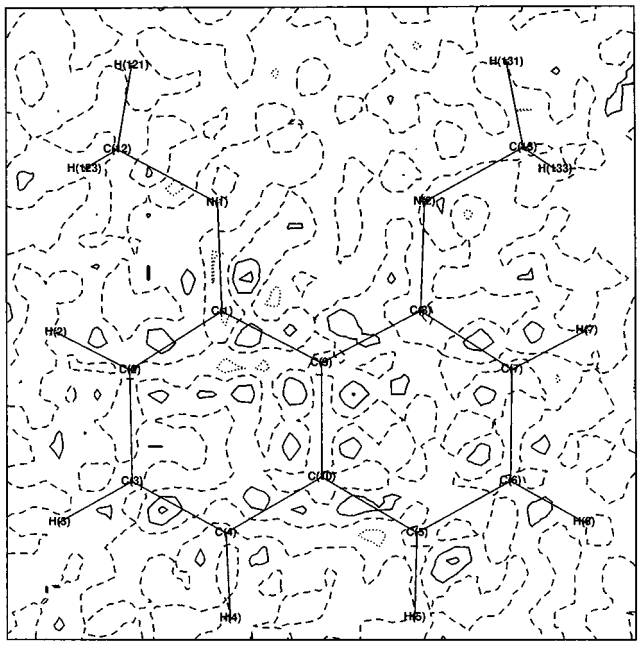

Figure 2. Residual density in the plane defined by C3, C6, C9. Contour interval = 0.1 eÅ^{-3}. Zero and negative contours are broken and dotted, respectively.

Figure 3 shows a composite section of the Laplacian distribution in sections fitting the approximately planar left and right-hand halves of the molecule. The program XDPROP of the XD package[34] was used to compute this and also to obtain a critical point (CP) analysis for the bonds. The bond paths (lines along which charge is concentrated and on which the CPs are situated) are depicted together with the charge densities ρ_b calculated at the bond critical points in Figure 4, and with Laplacian values $\nabla^2\rho_b$ in Figure 5. Slight curvatures of the bond paths C4−C10, C5−C6 are unexplained features. XDPROP computes errors of CP properties taking into account only errors from the multipole populations, not including coordinates and κ values. Hence the errors are underestimated, particularly for the rapidly changing Laplacian function. For this reason they have been omitted from Figure 5.

Hirshfeld's rigid bond test[42] was applied to the thermal parameters obtained from the refinement. It is supposed that

(33) Clementi, E; Roetti, C. *At. Data Nucl. Data Tables* **1974**, *14*, 177.
(34) Koritsanszky, T.; Howard, S. T.; Richter, T.; Mallinson, P. R.; Su, Z.; Hansen, N. K. *XD, a computer program package for multipole refinement and analysis of charge densities from X-ray diffraction data*, 1995.
(35) Blessing, R.H. *Acta Crystallogr.* **1995**, *B51*, 816.
(36) Wilson, C. C. in *Neutron Scattering Data Analysis 1990*; Johnson, M. W., Adam Hilger: Bristol, U.K., 1990; IoP Conference Series, Vol. 107, pp 145−163; Wilson, C.C. *J. Mol. Struct.* **1997**, *405*, 207.
(37) Brown, P. J.; Matthewman, J. C. *Rutherford Appleton Laboratory Report* **1993**, *RAL-93-009*.
(38) Becker, P.; Coppens, P. *Acta Crystallogr.* **1974**, *A30*, 129 and 148.
(39) Larsen, A.C.; von Dreele, R.B. *GSAS. Los Alamos Nat. Lab. Rep.* **1986**, LAUR 86.
(40) Sheldrick, G.M. *SHELXL93. Program for the Refinement of Crystal Structures.* University of Göttingen, Germany, 1993.
(41) *International Tables for Crystallography*; Wilson, A. J. C., Ed.; Kluwer: Dordrecht, 1992; *Vol. C*, Table 4.4.4.1, pp 383−391.

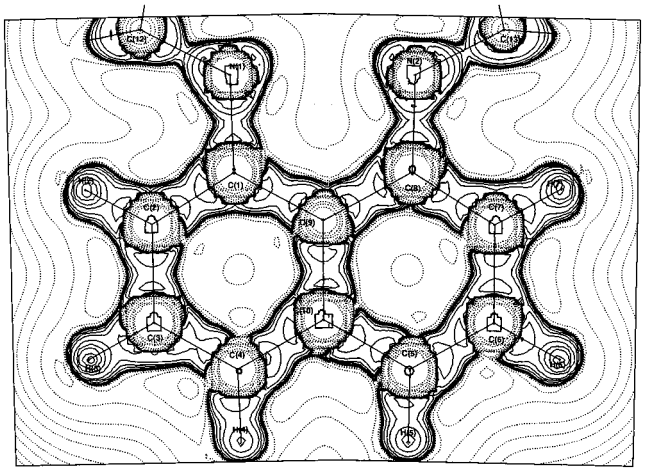

Figure 3. Laplacian map computed from the experimental multipole populations. Contours are drawn at logarithmic intervals in $-\nabla^2\rho/e\text{Å}^{-5}$. The map is a composite section defined by N1, C3, C10 for the left-hand moiety, and by N2, C10, C6 for the right-hand moiety.

the relative vibrational motion of a pair of covalently bonded atoms has an effectively vanishing component in the direction of the bond. If $z^2_{A,B}$ denotes the mean square displacement amplitude of atom A in the direction of atom B, then for every covalently bonded pair of atoms A and B

$$\Delta_{A,B} = z^2_{A,B} - z^2_{B,A} = 0$$

Three bonds have $\Delta_{A,B}$ values slightly greater than Hirshfeld's upper limit of 0.001 Å^2 for atoms at least as heavy as carbon, viz. C4−C10 0.0012, C6−C7 0.0016, N2−C13 0.0011 Å^2. Hirshfeld's analysis allows some tolerance in the acceptable limit. However, in view of this, together with the slightly higher than usual (for a first-row atom compound) range of residual density values, and errors up to 0.1 e on pseudoatom monopole charges, we take care not to over-interpret the results presented here.

Discussion

The asymmetric part of the DMAN crystal unit cell consists of one DMAN molecule (Figure 1) located in a general position. As a result, the two halves of the molecule interact with an asymmetric crystal environment although this is not apparent from an analysis of the low-temperature neutron or X-ray bond lengths and valence angles.[21] Nor can this asymmetry be seen in the monopole charges associated with potentially symmetry-related atoms of DMAN, nor in the charge density at bond critical points, ρ_b. Further, the ellipticity of bonds in the two halves of the DMAN molecule is insensitive to weak intermolecular interactions. Only at the level of the Laplacian of ρ at critical points, $\nabla^2\rho_b$, (Figure 5) do we see some differences between the values for potentially symmetrical bonds [−15.9(2) and −13.3(1) eÅ^{-5} for N1−C1 and N2−C8, −21.2(1) and −18.7(1) eÅ^{-5} for C3−C4 and C5−C6, −15.9(2) and −17.8(2) eÅ^{-5} for C3−H3 and C6−H6, respectively]. This small asymmetry of $\nabla^2\rho_b$ can also be seen in the shape of the contour lines in the Laplacian map calculated for the left and right aromatic rings of the naphthalene fragment (Figure 3). This can be taken as an indication of the magnitude of the effect of the weakest interactions on the valence-shell charge concentrations. For the cation, however, the asymmetry is much more pronounced as a result of the redistribution of charge on asymmetric protonation (also shown in Figure 5).

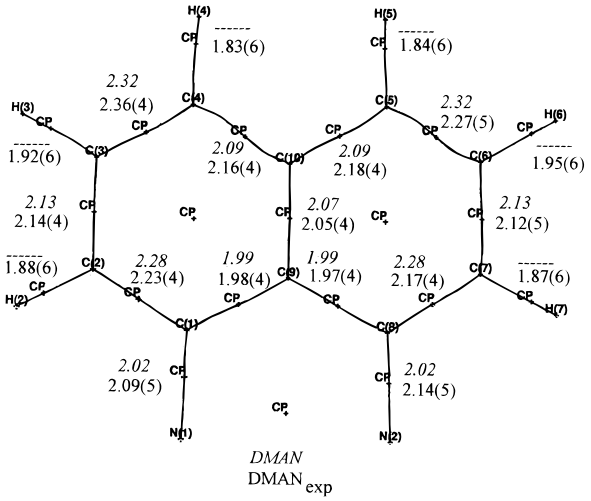

Figure 4. Bond paths, projected in the plane defined by C3, C6, C9, showing the locations of the critical points and values of $\rho_b/e\text{Å}^{-3}$. The values labelled DMAN are obtained from the ab initio theoretical calculation for the free base (ref 27).

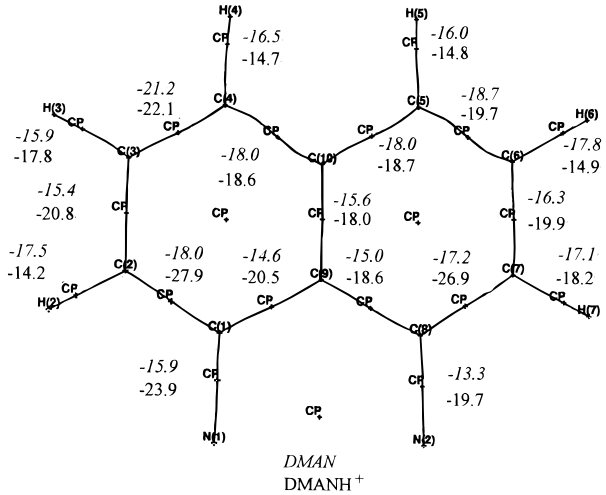

Figure 5. Experimental values of $\nabla^2\rho_b/e\text{Å}^{-5}$ for DMAN (italic) and its cation. Data for the latter are from ref 26.

It is noteworthy that despite such tiny differences between the left and the right parts of the DMAN molecule, separate signals are observed from potentially equivalent carbon nuclei in the solid state NMR and NQR spectra,[21,24,25] whereas such a well-defined perturbation as asymmetric hydrogen bonding in a series of DMANH$^+$ cations does not differentiate potentially equivalent carbon positions. This averaging of signals must be due to dynamic behaviour of the acidic proton, alternately occupying two positions at the N-atoms, the predominant position being observed in the time scale of X-ray and neutron diffraction methods.

Comparing critical point (CP) properties obtained in this study with those from our earlier work on the DMANH$^+$ cation,[26] we find that the C(aromatic)−N bonds show no difference in ρ_b; on average 2.12(5) eÅ^{-3} in the neutral DMAN molecule and 2.12(3) eÅ^{-3} in the cation. For the C−C bonds, there is a small (scarcely significant) increase in the average ρ_b on protonation: 2.15(4) eÅ^{-3} in DMAN, 2.24(3) eÅ^{-3} in DMANH$^+$. Some redistribution of electron density on protonation is also suggested by the lack of correlation between the DMAN and

(42) Hirshfeld, F. L. *Acta Crystallogr.* **1976**, *A32*, 239.

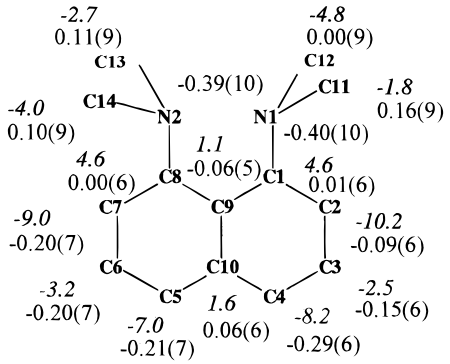

Figure 6. Chemical shift differences, δ(DMAN) − δ(DMANH$^+$) (/ppm, italic, from ref 15), and monopole charges (/e) for DMAN.

DMANH$^+$ cation experimental atomic charges. For example, the nitrogen atoms, nearest in the cation to the acidic proton and participating in the [N−H···N]$^+$ H-bond, have their negative charge reduced from −0.40(10) eÅ^{-3} in DMAN to −0.23(5) eÅ^{-3} in DMANH$^+$.[26]

The experimental atomic charges for DMAN are shown in Figure 6. The outer, protonated carbons are negative, as in DMANH$^+$. As noted previously,[26] protonation of DMAN to DMANH$^+$ causes de-shielding of the outer carbons as a result of migration of charge towards the positive charge of the proton. Hence the ^{13}C solid-state NMR chemical shifts for the outer carbons increase, and the difference δ(DMAN) − δ(DMANH$^+$) is negative. For DMANH$^+$ the monopole charges for the carbon atoms were found to correlate with these chemical shift differences, but for DMAN the correlation is much weaker.

The molecular structure of DMAN obtained from neutron diffraction closely resembles that from the earlier ab initio MO calculation,[27] with the biggest deviations of 0.022, 0.015, and 0.014 Å for C1−C2, N1−C1, and C3−C4 bond lengths, respectively. In the case of the bond angles the largest differences are between the C9−C1−N1 angles (ca. 1°). These differences are likely to be due to the inadequacy of the basis set used, the lack of electron correlation, and the fact that ab initio calculations do not take into account intermolecular interactions.

Consequences of protonation at the structural level are illustrated in Figure 7. From the figure we can see some systematic differences for the aromatic C−C bonds. On average the C−C bonds in the cation are shorter than in the free base (1.402 Å cf. 1.412 Å). This can be attributed to redistribution of electron density from the periphery of the moiety towards its center, effectively increasing the double bond character of the aromatic bonds. On the other hand there is a lengthening of the C−N bonds, nearest to the protonation site, from 1.438 Å for DMAN to 1.476 Å, reflecting the breaking, on protonation, of conjugation between the nitrogen lone pairs and the aromatic electron density. It is interesting that the aromatic C−H bonds also exhibit a clear trend (they are longer in the cation than in the neutral base, on average 1.073 and 1.091 Å for DMAN and DMANH$^+$, respectively). Even C−H bonds far from the acidic proton are affected. The aliphatic C−-H bonds, surprisingly, appear not to be affected by protonation.

In order to find some relations between CP parameters of the charge distribution and structural parameters obtained from neutron diffraction, we show some important correlations in Figures 8 and 9. Here ρ_b signifies electron density at a bond critical point, R_{xx} is a bond length, and R is a correlation coefficient. As in the previously reported case[26] of weak C−H·

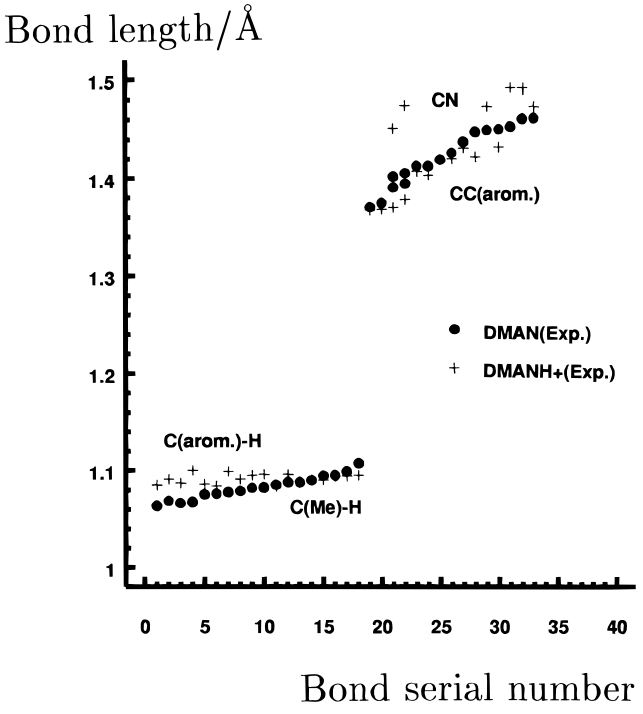

Figure 7. Distribution of C(ar)−H, C(Me)−H, C(ar)−C(ar), and C−N bond lengths (from neutron diffraction data). The dots are for DMAN and the crosses for DMANH$^+$ (data for the latter are from ref 14). The bonds are ordered from the shortest to the longest in DMAN.

··O hydrogen bonds, there are here quite strong relations between ρ_b and $\nabla^2\rho_b$ (Figure 8a), between $\nabla^2\rho_b$ and bond length (Figure 8b), and between ρ_b and bond length (Figure 8c), for covalent bonds. It can be seen that the slopes of such relations depend on the type of bond e.g. C−C and C−N. The largest difference in slopes is for the second of these relations, illustrating the high sensitivity of the Lapacian. This observation raises a question as to whether bond type-specific universal relationships might exist.

Some very interesting conclusions can be obtained from the correlation between CP parameters obtained from ab initio and experimental data for aromatic CC bonds of the naphthalene fragment of DMAN and the DMANH$^+$ cation. Let us concentrate on the strong dependence of ρ_b vs $\nabla^2\rho_b$ (Figure 9a). The experimental data show that on protonation of DMAN there is a decrease in the slope of this relation, from −0.056(7) for DMAN to −0.042(4) for the DMANH$^+$ cation (experimental graphs). Additionally, the data points are shifted on protonation towards higher values of ρ_b. The ab initio methods give different intercepts for both DMAN and its cation, although the slopes are similar to those obtained for the experimental data (−0.056 for both DMAN experimental and ab initio data, and −0.042 and −0.045 for DMANH$^+$ experimental and ab initio data, respectively). This systematic shift of the lines is perhaps an artefact of the ab initio calculations due to e.g., basis set inadequacy, lack of electron correlation, influence of the crystal lattice.

Similar relations can be obtained for $\nabla^2\rho_b$ *vs* C−C bond length (Figure 9b). In this case the slopes of the lines obtained for the experimental data differ significantly, whereas the ab initio lines (for DMAN and its cation) are almost overlapped. Both theoretical relations have slopes close to the experimental slope for the DMAN molecule. Hence the theoretical Laplacian values do not show the influence of protonation and also produce smaller intercepts. The large scatter of the data points for the

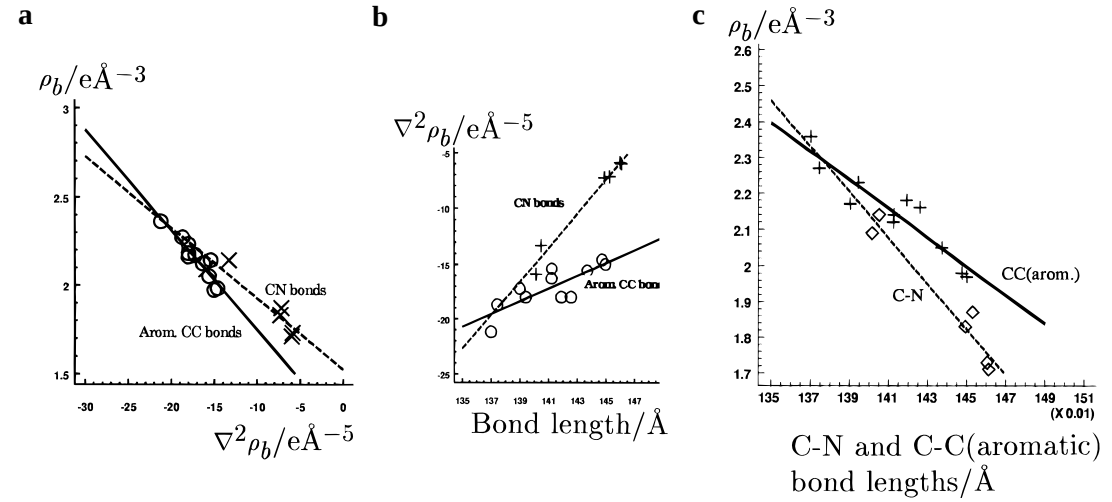

Figure 8. (a) Dependence of ρ_b on $\nabla^2\rho_b$ as a function of bond type, for DMAN experimental data: $\rho_b = -0.056(7)\nabla^2\rho_b + 1.2(1)$ (C−C bonds), R = −0.94; $\rho_b = -0.040(7)\nabla^2\rho_b + 1.52(7)$ (C−N bonds), $R = -0.94$. (b) Dependence of $\nabla^2\rho_b$ on bond length as a function of bond type, for DMAN experimental data: $\nabla^2\rho_b = 58(14)R_{CC} - 99(20)$, $R = 0.81$; $\nabla^2\rho_b = 152(12)R_{CN} - 228(18)$, $R = 0.99$. (c) Dependence of ρ_b on bond length as a function of bond type, for DMAN experimental data: (+ stands for C−C aromatic bonds, solid line, ◇ stands for CN bonds, dashed line): $\rho_b = -4.0(5)R_{CC} + 7.8(7)$, $R = -0.93$; $\rho_b = -6.4(8)R_{CN} + 11(1)$, $R = -0.97$.

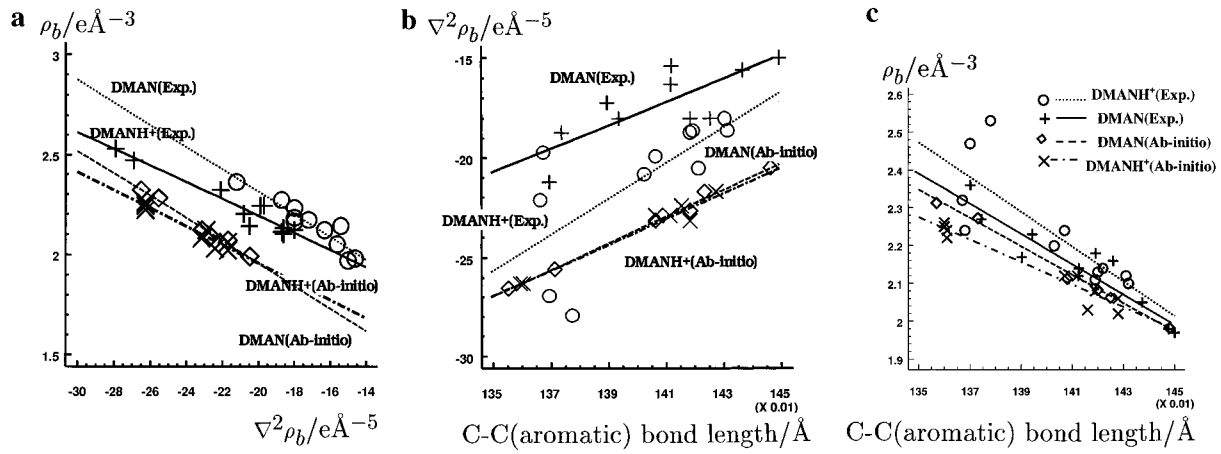

Figure 9. (a) Dependence of ρ_b on $\nabla^2\rho_b$ for DMAN experimental data: $\rho_b = -0.056(7)\nabla^2\rho_b + 1.2(1)$, $R = -0.94$; for $DMANH^+$ experimental data:[26] $\rho_b = -0.042(4)\nabla^2\rho_b + 1.34(9)$, $R = -0.96$; for DMAN ab initio data:[27] $\rho_b = -0.056(2)\nabla^2\rho_b + 0.83(4))$, $R = -0.995$; for $DMANH^+$ ab initio data:[27] $\rho_b = -0.045(4)\nabla^2\rho_b + 1.0(1)$, $R = -0.96$. (b) Dependence of $\nabla^2\rho_b$ on bond length for DMAN experimental data: $\nabla^2\rho_b = 58(14)R_{CC} - 99(20)$, $R = 0.81$; for $DMANH^+$ experimental data:[26] $\nabla^2\rho_b = 90(31)R_{CC} - 147(43)$, $R = 0.69$; for DMAN ab initio data:[27] $\nabla^2\rho_b = 66(2)R_{CC} - 117(2)$, $R = 0.997$; for $DMANH^+$ ab initio data:[27] $\nabla^2\rho_b = 64(4)R_{CC} - 113(21)$, $R = 0.98$. (c) Dependence of ρ_b on bond length for DMAN experimental data: $\rho_b = -4.0(5)R_{CC} + 7.8(7)$, $R = -0.93$; for $DMANH^+$ experimental data:[26] $\rho_b = -4.6(1)R_{CC} + 8.7(2)$, $R = -0.81$; for DMAN ab initio data:[27] $\rho_b = -3.75(9)R_{CC} + 7.4(1)$, $R = -0.997$; for $DMANH^+$ ab initio data:[27] $\rho_b = -3.0(3)R_{CC} + 6.3(4)$, $R = -0.93$.

$DMANH^+$ cation reflects the previously discussed asymmetry of the Laplacian, consequent upon $[N-H\cdots N]^+$ hydrogen bonding.

Rather different relations are found for ρ_b *vs* aromatic C−C bond lengths (Figure 9c). In this case the ab initio results can differentiate the DMAN base and its cation although they again underestimate the experimental data. It is interesting that the difference between the ρ_b values is a function of C−C bond length. It decreases when the C−C bond length increases. Furthermore, the DMAN molecule is better described by the ab initio results than is the cation. This larger discrepancy between experiment and theory for the shortest, close to double, bonds implies some inadequacy of either the multipole model or the ab initio calculation, or both, when the results are analysed at this very detailed level.

Despite a number of close contacts existing between methyl hydrogen atoms and aromatic carbons in neighboring molecules, we find only two critical points. These are situated between H113 and C9, and between H133 and C3, where both carbon atoms are generated by the symmetry operation $^1/_2 - x, -y, -^1/_2 + z$. Figure 10 shows curved interaction lines characterising these two contacts, as well as the interaction line passing through the lone pairs on N1 and N2, and linking these nuclei. The H−C(ar) interaction lines are curved close to the hydrogens, and are almost perpendicular to the aromatic rings, which is consistent with CH$\cdots\pi$-electron interactions.

Conclusions

In this first study of an uncomplexed proton sponge compound, we find a small degree of asymmetry of the naphthalene moiety, induced by weak, asymmetric intermolecular interactions. The only manifestation of this asymmetry is at the level of the Laplacian of the charge distribution.

Comparing the DMAN molecule with its cation allows us to investigate the consequences of protonation. Atomic charges and structural parameters such as C−C, C−N and C−H bond lengths are affected. The C−C bonds are shortened, while C−N

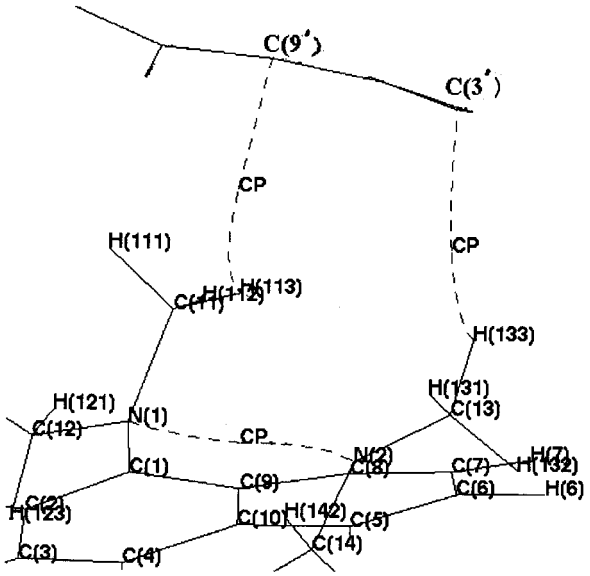

Figure 10. An illustration of N···N and CH···π-electron interaction lines. The upper fragment is part of the molecule generated by the symmetry operation $^1/_2 - x, -y, -^1/_2 + z$.

and C(ar)−H are lengthened. These changes are reflected in some CP properties, ρ_b for C−C bonds being on average larger in the cation than in the neutral molecule. The greatest effect on monopole charges is for the nitrogen atoms, which are much less negative in the cation.

There are some relationships between CP and structural parameters; ρ_b *vs* Laplacian, Laplacian *vs* bond length, and ρ_b *vs* bond length. They each depend on bond type, and are different for DMAN and its cation. Comparison with ab initio calculated values reveals some systematic discrepancies, the nature of which depends on the type of relationship.

Only two critical points are located between stacked DMAN molecules. Curved interaction lines can be associated with CH···π-electron interactions.

Acknowledgment. K.W. is grateful to the Department of Chemistry, University of Warsaw, for partial support from the project 12-501-07-BW-1383/41/98. Beam time allocation by ISIS (Chilton, U.K.) under RB/6795 SXD is gratefully acknowledged. We also thank the U.K. EPSRC for a graduate studentship (for K.L.McC), a fellowship (for D.S.Y.), and the Royal Society and the Polish Academy of Sciences for enabling P.R.M. and K.W. to participate in the European Science Exchange Programme.

Supporting Information Available: Fractional atomic coordinates and anisotropic displacement parameters, monopole charges, κ' and κ'' values obtained from the refinement, critical point data, multipole population coefficients, definitions of local axes, bond lengths and angles calculated from the multipole refinement and from the refinement with neutron diffraction data (PDF). This material is available free of charge via the Internet at http://pubs.acs.org.

JA983393Z